Primitive Equations Under Location Uncertainty: Analytical Description and Model Development

Francesco Tucciarone, Etienne Mémin, Long Li

Primitive Equations Under Location Uncertainty: Analytical Description and Model Development

Francesco L. Tucciarone, Etienne Mémin, and Long Li

Abstract Resolving numerically all the scale interactions of ocean dynamics in a high resolution realistic configuration is today far beyond reach, and only large scale representations can be afforded. In this work, we study a stochastic parameterization of the ocean primitive equations derived within the modelling under location uncertainty framework. First numerical assessments built with the NEMO core's code are provided for a double-gyres configuration.

Keywords Stochastic parametrization · Ocean modelling

1 Introduction

The Ocean covers a major part of Earth's surface and has an important stabilizing effect on the climate. For climatic prediction, accurate likely ensemble forecasts of future ocean states are consequently essential. However, due to an evident computational limitation high resolution simulations are completely unfeasible and only large-scale ocean representations can be handled. To face this difficulty, and the need of generating different likely future scenarios, there has been a growing interest in the geophysical sciences to set up flow models that incorporate in their dynamics noise terms related to uncertainties or errors. In accounting for the actions of unresolved processes in a random way, these stochastic models are in general less diffusive than the classical large-scale deterministic models. The unresolved processes include small-scale turbulence effects, boundary value uncertainties or uncertainties coming either from scale coarsening or from the numerical schemes used. Moreover, compared to classical large-scale deterministic modelling, the additional degree of freedom brought by the stochastic component allows us to devise new intermediate models [4, 3, 6, 7, 8]. The addition of noise in fluid

F. L. Tucciarone (✉) · E. Mémin · L. Li
INRIA Rennes Bretagne Atlantique, IRMAR – UMR CNRS 6625, Rennes, France
e-mail: francesco.tucciarone@inria.fr; etienne.memin@inria.fr; long.li@inria.fr

B. Chapron et al. (eds.), *Stochastic Transport in Upper Ocean Dynamics*,
Mathematics of Planet Earth 10, https://doi.org/10.1007/978-3-031-18988-3_18

dynamics models cannot be done in a haphazard manner. Ad-hoc choices for model noise can fundamentally perturb the corresponding fluid dynamics models, making them exhibit unrealistic properties [3]. Rigorously justified methodologies for choosing the model noise have recently been introduced by Mémin [1] and Holm [2]. These derivations lead to large classes of stochastic geophysical fluid dynamics models that preserve either energy or circulation, respectively. Such models naturally emerge from a decomposition of the flow velocity field in terms of a smooth component and a time uncorrelated uncertainty random term. This decomposition is reminiscent, in spirit, of the classical Reynolds decomposition, and enables the definition of large-scale representation with a stochastic term representing small-scale effects. The Location Uncertainty (LU) formulation has been found to be more accurate in structuring the large-scale flow [4] and in reproducing long-terms statistics [22] for the barotropic quasi-geostrophic model. It also provides a good trade-off between model error representation and ensemble spread [21, 23] for the rotating shallow water model and the surface quasi-geostrophic model. In this work we explore more specifically a stochastic version of the primitive equations, named primitive equations under Location Uncertainty. The derivation of this model is detailed and first numerical experiments built from the NEMO code are assessed.

2 Location Uncertainty (LU)

In the LU formalism, the Lagrangian displacement $\mathbf{X}_t$ associated to a fluid particle is decomposed as:

$$\mathbf{X}_t\left(\mathbf{x}\right) = \mathbf{X}_{t_0}\left(\mathbf{x}\right) + \int_0^t \mathbf{v}\left(\mathbf{X}_s\left(\mathbf{x}\right), s\right) \mathrm{d}s + \int_0^t \boldsymbol{\sigma}\left(\mathbf{X}_s\left(\mathbf{x}\right), s\right) \mathrm{d}\mathbf{B}_s, \tag{1}$$

where $\mathbf{X}\colon \Omega \times \mathbb{R}^+ \to \Omega$ is the fluid flow map, that is the trajectory followed by fluid particles starting at initial map $\mathbf{X}|_{t=0}\left(\mathbf{x}\right) = \mathbf{x}_0$ of the bounded domain $\Omega \subset \mathbb{R}^3$. Written in differential form Eq. (1) takes the usual form:

$$\mathrm{d}\mathbf{X}_t\left(\mathbf{x}_0\right) = \mathbf{v}\left(\mathbf{X}_t, t\right)\, \mathrm{d}t + \boldsymbol{\sigma}\left(\mathbf{X}_t, t\right) \mathrm{d}\mathbf{B}_t. \tag{2}$$

The first component, $\mathbf{v}\left(\mathbf{X}_t, t\right)$, represents the smooth, resolved velocity field of the flow. It corresponds to the integration of the equations of motions, solved on a grid of a given resolution, and it is supposed to be both spatially and temporally correlated. The second term, $\boldsymbol{\sigma}\left(\mathbf{X}_t, t\right) \mathrm{d}\mathbf{B}_t$, is a stochastic process that assembles the unresolved flow component, uncertainties on the flow and turbulent effects. This stochastic contribution, often referred to as *noise* in the following, is built from the application of an Hilbert-Schmidt kernel integral operator, $\boldsymbol{\sigma}$, to an I_3-cylindrical Wiener process $\mathbf{B}$

$$(\boldsymbol{\sigma}\,(\mathbf{X}_t, t)\,\mathrm{d}\mathbf{B}_t)^i = \int_{\Omega} \breve{\sigma}_{ik}\,(\mathbf{X}_t, \mathbf{y}, t)\,\mathrm{d}\mathrm{B}_t^k\,(\mathbf{y})\,\mathrm{d}\mathbf{y}, \tag{3}$$

where $\mathbf{B}$ is defined on a filtered probability space $\{\Omega, \mathcal{F}, \mathrm{P}, (\mathcal{F}_t)_t\}$ and $(\mathcal{F}_t)_t$ is the filtration adapted to $\mathbf{B}$. The application of the (integrable) kernel $\breve{\sigma}$ imposes fast/small scales spatial correlation and defines a centered Gaussian process $\boldsymbol{\sigma}\mathrm{d}\mathbf{B}_t \sim \mathcal{N}(0, \mathbf{Q}\mathrm{d}t)$, with covariance tensor defined as

$$\begin{aligned} Q_{ij}\,(\mathbf{x}, \mathbf{y}, t, s) &= \mathbb{E}\left[(\boldsymbol{\sigma}\,(\mathbf{x}, t)\,\mathrm{d}\mathbf{B}_t)^i\,(\boldsymbol{\sigma}\,(\mathbf{y}, s)\,\mathrm{d}\mathbf{B}_s)^j\right] \\ &= \delta\,(t-s)\,\mathrm{d}t \int_{\Omega} \breve{\sigma}_{ik}\,(\mathbf{x}, \mathbf{z}, t)\,\breve{\sigma}_{kj}\,(\mathbf{z}, \mathbf{y}, s)\;\mathrm{d}\mathbf{z}. \end{aligned}$$

The strength of the noise is measured by the diagonal components of the covariance tensor per unit of time, i.e. the variance tensor, $\mathbf{a}$, defined as $\mathbf{a}(\mathbf{x}, t)\delta(t - t')\mathrm{d}t = \mathbf{Q}(\mathbf{x}, \mathbf{x}, t, t')$. The variance tensor is symmetric and positive definite at any point $\mathbf{x}$ of the domain. Notably, it has the dimension of a viscosity in $\mathrm{m}^2\mathrm{s}^{-1}$. The covariance operator is self-adjoint, positive definite and compact and admits a convenient spectral decomposition.

In this paper, the noise will always be assumed to be centred, but it can be proven through Girsanov theorem that one can redefine the Lagrangian displacement (2) as

$$\mathrm{d}\mathbf{X}_t\,(\mathbf{x}_0) = [\mathbf{v}\,(\mathbf{X}_t, t) - \boldsymbol{\mu}_t\,(\mathbf{X}_t)]\,\mathrm{d}t + \boldsymbol{\sigma}\mathrm{d}\widetilde{\mathbf{B}}_t\,(\mathbf{X}_t)\,, \tag{4}$$

where the Wiener process $\widetilde{\mathbf{B}}_t$ is a centred process under a new probability measure Q drifted by $\boldsymbol{\mu}_t$. Indeed a non centred Wiener process shifted by a random process $(\mathbf{Y}_t)_t$ can be defined as:

$$\widetilde{\mathbf{B}}_t = \mathbf{B}_t + \int_0^t \mathbf{Y}_s\,\mathrm{d}s. \tag{5}$$

Under good properties of $(\mathbf{Y})_t$ ($\mathcal{F}_t$-measurability, almost sure L^2-integrability and Novikov condition) there exists a measure Q such that $(\widetilde{\mathbf{B}}_t)_t$ is a Q$-$ Wiener process With the non centred random process $\widetilde{\mathbf{B}}_t$ we can rewrite the equations with respect to $\widetilde{\mathbf{B}}_t$ as

$$\boldsymbol{\sigma}\mathrm{d}\mathbf{B}_t\,(\mathbf{X}_t) = \boldsymbol{\sigma}\mathrm{d}\widetilde{\mathbf{B}}_t\,(\mathbf{X}_t) - \boldsymbol{\sigma}\,(\mathbf{X}_t, t)\,\mathbf{Y}_t\,\mathrm{d}t. \tag{6}$$

Denoting $\boldsymbol{\sigma}\,(\mathbf{X}_t, t)\,\mathbf{Y}_t$ as $\boldsymbol{\mu}_t$ one can write the Lagrangian displacement (2) as (4) and under Q the Wiener process $\mathrm{d}\widetilde{\mathbf{B}}_t$ is centred thus the writing of $\mathrm{d}\mathbf{X}_t$ has the same form as (2) but under a new measure. All the arguments provided in the following will hold for this process under Q. The use of a drifted noise $\boldsymbol{\sigma}\mathrm{d}\widetilde{\mathbf{B}}_t$ is fundamental when the processes employed to operationally define the noise are not centred, hence displaying a non-zero time average.

3 Stochastic Transport Theorem

The derivation of Eulerian flow dynamics models within the LU formalism relies on a stochastic version of the Reynolds transport theorem (SRTT), introduced in [1], which describes the rate of change of a random scalar q transported by the stochastic flow (2) within a flow volume V_t:

$$\mathrm{d}\int_{V_t} q\,(\mathbf{x},t)\;\mathrm{d}\mathbf{x} = \int_{V_t} \left\{\mathrm{D}_t q + q\nabla\cdot\left[\mathbf{v}^\star\,\mathrm{d}t + \boldsymbol{\sigma}\,\mathrm{d}\mathbf{B}_t\right]\right\}(\mathbf{x},t)\;\mathrm{d}\mathbf{x}, \tag{7}$$

with the operator

$$\mathrm{D}_t q = \mathrm{d}_t q + \left[\mathbf{v}^\star\,\mathrm{d}t + \boldsymbol{\sigma}\,\mathrm{d}\mathbf{B}_t\right]\cdot\nabla q - \frac{1}{2}\nabla\cdot(\mathbf{a}\nabla q)\;\mathrm{d}t, \tag{8}$$

defining the stochastic transport operator. The SRTT is in perfect analogy with the deterministic Reynolds transport theorem (compare with [13] section 5.3), and the various terms can be interpreted physically. Proceeding in order, the first right-hand side term of (8) is the *increment in time* at a fixed location of the process q, that is $\mathrm{d}_t q = q\,(\mathbf{X}_t, t+\mathrm{d}t) - q\,(\mathbf{X}_t, t)$. This contribution plays the role of the partial time derivative for a process that is not time differentiable. The term enclosed in the square brackets is a *stochastic advection displacement*. It involves a time correlated modified advection,

$$\mathbf{v}^\star = \mathbf{v} - \frac{1}{2}\nabla\cdot\mathbf{a} + \boldsymbol{\sigma}^{\mathrm{T}}\,(\nabla\cdot\boldsymbol{\sigma})\,, \tag{9}$$

and a fast evolving, time uncorrelated noise $\boldsymbol{\sigma}\,\mathrm{d}\mathbf{B}_t$. The advection by this term of variable q leads to a *multiplicative noise*, which is hence non Gaussian. This type of noise is often denoted as *transport noise* in the literature. The second term of the modified advection is coined as the *Ito-Stokes drift* velocity in [4], $\mathbf{v}_s = \frac{1}{2}\nabla\cdot\mathbf{a}$. It represents an effective transport velocity resulting from statistical effects due to inhomogeneities of the noise term. The last term of the transport operator is a dissipation term that depicts the mixing mechanism due to the unresolved scales. Following [5] one can consider the transport of a characteristic function to introduce an evolution equation for the Jacobian determinant J of the flow:

$$\mathrm{D}_t J - J\nabla\cdot\left[\left(\mathbf{v} - \mathbf{v}^s + \boldsymbol{\sigma}^{\mathrm{T}}\,(\nabla\cdot\boldsymbol{\sigma})\right)\mathrm{d}t + \boldsymbol{\sigma}\,\mathrm{d}\mathbf{B}_t\right] = 0. \tag{10}$$

This equation provides a clear condition for the stochastic flow to be isochoric:

$$\nabla\cdot\left[\mathbf{v}^\star\,\mathrm{d}t + \boldsymbol{\sigma}\,\mathrm{d}\mathbf{B}_t\right] = 0. \tag{11}$$

4 Boussinesq Equations

Under location uncertainty, a stratified ocean can be modelled with a modified version of Boussinesq equations. The derivation that is outlined here follows almost verbatim the asymptotic derivation given in [12]. First, one applies the SRTT (7) to the density and imposes conservation, that is $\mathrm{d}\int_{V_t}\rho\left(\mathbf{x},t\right)\,\mathrm{d}\mathbf{x}=0$. Then, assuming that the fluctuations of density are small compared to the mean,

$$\rho\left(\mathbf{x},t\right)=\rho_0\left[1+\varepsilon\,\delta\hat{\rho}\left(t,\mathbf{x}\right)\right], \tag{12}$$

and using ε as an asymptotic ordering parameter to perform an expansion of the conservation of mass, the first order is found to be:

$$\nabla\cdot\left[\mathbf{v}^{\star}\,\mathrm{d}t+\boldsymbol{\sigma}\,\mathrm{d}\mathbf{B}_t\right]=0, \tag{13}$$

that can be split in two incompressibility conditions involving both the modified drift velocity $\mathbf{v}^{\star}$ and the fast scale component $\boldsymbol{\sigma}\,\mathrm{d}\mathbf{B}_t$ thanks to the uniqueness of semi-martingale decomposition [15]. Applying again the SRTT (7) to the momentum reads

$$\rho\mathrm{D}_t\mathbf{v}=-\nabla\left(p-\frac{\mu}{3}\nabla\cdot\mathbf{v}\right)\,\mathrm{d}t-\nabla\left(\mathrm{d}p_t^{\sigma}\right)-\rho g\mathbf{e}_3\,\mathrm{d}t, \tag{14}$$

where the right hand side entails pressure forces, compressibility effects [14] and gravitational forces. The compressibility term $\frac{\mu}{3}\nabla\cdot\mathbf{v}$, with μ dynamical viscosity of water, is usually neglected in the deterministic derivation of the Boussinesq model, but in this model is maintained in view of the different incompressibility condition (12), that enforces $\nabla\cdot\mathbf{v}=\nabla\cdot\mathbf{v}_s$. Following classical nondimensionalization procedure [12, 14], characteristic scales are introduced as:

$$\mathbf{x}=L\hat{\mathbf{x}},\qquad\mathbf{v}=U\hat{\mathbf{v}},\qquad t=\tau\hat{t},\qquad p=\frac{\rho_0U^2}{\epsilon}\hat{p},\qquad g=\frac{U^2}{\epsilon L}\hat{g}, \tag{15}$$

with $\tau=L/U$ advective time scale. Furthermore, the variance tensor is assumed to scale as $\mathbf{a}=A\hat{\mathbf{a}}$ so that the fast-evolving component $\boldsymbol{\sigma}\,\mathrm{d}\mathbf{B}_t$ and the kernel $\boldsymbol{\sigma}$ can be scaled as

$$\boldsymbol{\sigma}\,\mathrm{d}\mathbf{B}_t=\sqrt{\frac{AL}{U}}\hat{\boldsymbol{\sigma}}\,\mathrm{d}\hat{\mathbf{B}}_t\quad\text{and}\quad\boldsymbol{\sigma}=\sqrt{A}\hat{\boldsymbol{\sigma}}. \tag{16}$$

In this novel framework a non-dimensional parameter $\Upsilon=UL/A$ is introduced to compare advection and stochastic diffusion terms in the momentum equation. This parameter is termed *stochastic Peclet number*, in perfect similarity with the deterministic advection-diffusion problem [10]. Introducing these variables, following [12], one obtains:

$$\rho_0\left(1+\epsilon\delta\hat{\rho}\right)\ \left\{\mathrm{d}_t\hat{\mathbf{v}}+\left[\left(\hat{\mathbf{v}}\ -\ \frac{1}{\Upsilon}\hat{\mathbf{v}}_s\right)\mathrm{d}\hat{t}+\frac{1}{\Upsilon^{1/2}}\hat{\boldsymbol{\sigma}}\,\mathrm{d}\hat{\mathbf{B}}_t\right]\cdot\hat{\nabla}\hat{\mathbf{v}}\right.$$
$$\left.-\ \frac{1}{2\Upsilon}\hat{\nabla}\cdot\left(\hat{\mathbf{a}}\hat{\nabla}\hat{\mathbf{v}}\right)\,\mathrm{d}\hat{t}\right\}=\hat{\nabla}\left(-\frac{\rho_0}{\epsilon}\hat{p}+\frac{1}{\mathrm{Re}\Upsilon}\frac{1}{3}\hat{\nabla}\cdot\hat{\mathbf{v}}_s\right)\,\mathrm{d}\hat{t}\quad(17)$$
$$-\hat{\nabla}\left(\frac{P^\sigma}{U^2}\mathrm{d}\hat{p}_t^\sigma\right)-\rho_0\left(1+\epsilon\delta\hat{\rho}\right)\frac{\hat{g}}{\epsilon}\mathbf{e}_3\,\mathrm{d}\hat{t}.$$

Expanding each variable as an asymptotic with ϵ taken as ordering parameter, Eq. (17) provides at lowest order, once dimensional variables are replaced to non-dimensional variables,

$$\nabla p_0=-\rho_0 g\mathbf{e}_z,\quad p_0\left(z\right)=-\rho_0 g z.\tag{18}$$

Decomposing the density into a background constant density and a deviation, corresponds on the pressure variable to a decomposition in terms of a hydrostatic component and a pressure fluctuation. This splitting,

$$\rho\left(t,\mathbf{x}\right)=\rho_0+\rho'\left(t,\mathbf{x}\right),\qquad p\left(t,\mathbf{x}\right)=p_0+p'\left(t,\mathbf{x}\right),\tag{19}$$

allows the recognition of the first order component of the pressure as the deviation from the hydrostatic pressure p', so that Eq. (17) at first order in dimensional form becomes

$$\mathrm{d}_t\mathbf{v}+\left[\left(\mathbf{v}-\mathbf{v}^s\right)\,\mathrm{d}t\ +\boldsymbol{\sigma}\,\mathrm{d}\mathbf{B}_t\right]\cdot\nabla\mathbf{v}-\frac{1}{2}\nabla\cdot\left(\mathbf{a}\nabla\mathbf{v}\right)\,\mathrm{d}t=$$
$$=\nabla\left(-p'+\frac{\nu}{3}\nabla\cdot\mathbf{v}_s\right)\,\mathrm{d}t-\nabla\left(\frac{dp_t^\sigma}{\rho_0}\right)-\frac{\rho'}{\rho_0}g\mathbf{e}_z\,\mathrm{d}t.$$

The splitting (19) also introduces naturally the *buoyancy* $\mathbf{b}=-g\mathbf{e}_3\rho'\left(t,\mathbf{x}\right)/\rho_0$ in the equations of motions, representing the upward (or downward) force associated with the density anomaly ρ'. In terms of buoyancy, the momentum equation can be written as

$$\mathrm{D}_t\mathbf{v}=\nabla\left(-p'-\frac{dp_t^\sigma}{\rho_0}+\frac{\nu}{3}\nabla\cdot\mathbf{v}_s\right)\,\mathrm{d}t-\mathbf{b}\,\mathrm{d}t.\tag{20}$$

A stochastic transport equation can be written for the buoyancy from mass conservation. However, in this work a tracer transport equation on salinity, S, and temperature, T, is preferred, relating then the buoyancy and the tracers with a buoyancy state equation $b=b\left(T,S,z\right)$. The conservation of a given tracer θ is expressed as

$$\mathrm{D}_t\theta+\theta\nabla\cdot\left[\left(\mathbf{v}-\mathbf{v}_s\right)\,\mathrm{d}t+\boldsymbol{\sigma}\,\mathrm{d}\mathbf{B}_t\right]=F^\theta\,\mathrm{d}t+D^\theta\,\mathrm{d}t,\tag{21}$$

where the variation of tracer quantity is balanced by a forcing term F^θ and a diffusive term D^θ. We note that here these terms are assumed to be regular in time, although additional Brownian terms could be considered to encode intermittent forcing. The resulting system, split into horizontal and vertical equations using the convention $\mathbf{v} = (\mathbf{u}, w)$, is:

Horizontal momentum:

$$\mathrm{D}_t\mathbf{u} + f\mathbf{e}_3 \times \left(\mathbf{u}\,\mathrm{d}t + \frac{1}{2}\boldsymbol{\sigma}\,\mathrm{d}\mathbf{B}_t^{\mathrm{H}}\right) = \nabla_{\mathrm{H}}\left(-p' + \frac{\nu}{3}\nabla\cdot\mathbf{v}\right)\mathrm{d}t - \nabla_{\mathrm{H}}\mathrm{d}p_t^\sigma \quad (22)$$

Vertical momentum:

$$\mathrm{D}_t w = \frac{\partial}{\partial z}\left(-p' + \frac{\nu}{3}\nabla\cdot\mathbf{v}\right)\mathrm{d}t - \frac{\partial}{\partial z}\mathrm{d}p_t^\sigma + b\,\mathrm{d}t \quad (23)$$

Temperature and salinity:

$$\mathrm{D}_t T = \kappa_T \Delta T\,\mathrm{d}t, \quad (24)$$

$$\mathrm{D}_t S = \kappa_S \Delta S\,\mathrm{d}t, \quad (25)$$

Incompressibility:

$$\nabla\cdot\left[\mathbf{v} - \mathbf{v}^s\right] = 0, \qquad \nabla\cdot\boldsymbol{\sigma}\,\mathrm{d}\mathbf{B}_t = 0, \quad (26)$$

Equation of state:

$$b = b\,(T, S, z)\,. \quad (27)$$

Temperature and salinity are introduced as active tracers, as they modify the buoyancy field, and their stochastic evolution is obtained again by application of the SRTT (7), balanced with a diffusion process with diffusivity κ_T and κ_S respectively. The unusual coefficient $1/2$ in the random Coriolis term can be shown to appear naturally from a derivation of the non-inertial acceleration in this stochastic framework, again following the derivation of [12]. Metric terms relative to the rotation of the earth should also be adapted to the stochastic Frenet-Serret formula $\mathrm{d}\mathbf{C} = \boldsymbol{\Omega}\mathrm{d}t \times \mathbf{C}$ in the case of planetary scale simulations. In Eqs. (22) and (23) the *stochastic pressure* is introduced, and corresponds to a zero-mean turbulent pressure related to the small scale velocity component (i.e. noise). It is a martingale term. An operational model referred to as the primitive equations can be obtained through the so-called hydrostatic balance, resulting from neglecting the vertical acceleration terms through a proper scaling of the velocity. In our stochastic setting, the vertical momentum equation reads, after neglecting the large scale acceleration terms and for moderate noise ($\Upsilon \sim \mathcal{O}(1)$ so as the martingale terms related to the vertical velocity component are negligible):

$$-\frac{\partial p'}{\partial z} + b = 0 \quad \text{and} \quad \frac{\partial \mathrm{d}p_t^\sigma}{\partial z} = 0, \quad (28)$$

where the bounded variation terms and the martingale terms have been safely separated. The left equation constitutes the usual hydrostatic balance. With the scaling used, the stochastic pressure is constant along depth and is in balance with the stochastic Coriolis component [9, 5]. These two martingale terms can be removed then from the horizontal momentum equation. In this setting the vertical component of the momentum equation becomes a diagnostic component that can be recovered integrating the continuity equation given by (26). In a similar way, the large scale pressure is obtained from the vertical integration of the hydrostatic relation. The scaling parameter Υ can also be related to the ratio between the Mean Kinetic Energy (TKE) when an advective time scale is used, that is

$$\Upsilon = \frac{U^2}{A/\tau} = \frac{1}{\epsilon}\frac{MKE}{TKE} \tag{29}$$

where $\epsilon = \tau_\sigma/\tau$, is the ratio of the fast-scale to the slow-scale correlation times. This ratio can be adapted to the different variables involved (i.e. momentum, temperature or salinity) with a value similar to the inverse of the Schmidt number (ratio of diffusion rates) making hence the noise scaling parameter, Υ, dependant on the variable transported. The parameter Υ appears in dimensional analysis and asymptotic expansions, but plays also a paramount role in the quantification of the strength of the noise.

5 Methods

The experiments are performed with the level-coordinate free-surface primitive equation ocean model NEMO [16]. The domain configuration is a double-gyre configuration consisting of a 45° rotated beta plane centred at $\sim$ 30°N, 3180 km long, 2120 km wide and 4 km deep. The domain is bounded by vertical walls and a flat bottom. The seasonally varying wind and buoyancy forcings induce a strong jet to appear diagonally in the domain, separating a warm sub-tropical gyre from a cold sub-polar gyre. Three experiments were performed: two purely deterministic simulations at different resolutions, 1/27° (R27d) and 1/3° (R3d), and one stochastic simulation at 1/3° (R3LU). Each simulation was run for 10 years with data collected every (and averaged over) 5 days. The focus of this paper is to assess the benefits brought by LU to the coarse simulation, so the parameters of the simulation were chosen following thoroughly [17, 18] (see Table 1 for an overview of their values). In this first study, we restrict ourselves to 3D divergence-free horizontal noise (i.e. with no vertical component). In spectral form the random field and the variance tensor can be written as:

$$\boldsymbol{\sigma}\,\mathrm{d}\mathbf{B}_t = \sum_{i\in\mathbb{N}} \lambda_i^{1/2}\boldsymbol{\varphi}_i(\mathbf{x})\mathrm{d}\beta_t^i, \qquad \mathbf{a} = \sum_{i\in\mathbb{N}} \lambda_i \boldsymbol{\varphi}_i(\mathbf{x})\boldsymbol{\varphi}_i^{\mathrm{T}}(\mathbf{x}), \tag{30}$$

Table 1 Parameters of the model experiments

	R27d	R3d	R3LU
Horizontal resolution	1/27° (3.9 km)	1/3° (35.3 km)	1/3° (35.3 km)
Horizontal grid points	540×810	60×90	60×90
Vertical levels	30	30	30
Time step	5 min	20 min	20 min
Eddy viscosity	$-5\times10^{-9}\,\mathrm{m^4 s^{-1}}$	$-10^{-12}\,\mathrm{m^4 s^{-1}}$	$-10^{-12}\,\mathrm{m^4 s^{-1}}$
Eddy diffusivity	$-5\times10^{-10}\,\mathrm{m^4 s^{-1}}$	$300\,\mathrm{m^2 s^{-1}}$	$300\,\mathrm{m^2 s^{-1}}$

where $\{\boldsymbol{\varphi}_i(\mathbf{x}), i \in \mathbb{N}\}$ are the orthonormal eigenfunctions of the covariance operator associated to $\{\lambda_i, i \in \mathbb{N}\}$, the (real, positive) eigenvalues ranged in decreasing value order and $\{\beta_t^i, i \in \mathbb{N}\}$ is a set of standard (scalar) Brownian variables. This representation corresponds to the Karhunen-Loeve decomposition [24]. Operationally, the (finite) set of eigenfunctions $\{\boldsymbol{\phi}_i(\mathbf{x}), i \in [1, N]\}$ and of eigenvalues $\{\lambda_i, i \in [1, N]\}$ are computed through a proper orthogonal decomposition (POD) [11] of the temporal fluctuations of the two-dimensional low resolution residual $\mathbf{u}_{\mathrm{LR}}$. This velocity residual is obtained through Gaussian filtering of the high resolution deterministic simulation R27d, $\mathbf{u}_{\mathrm{LR}} = (1 - \mathcal{G})\,\mathbf{u}_{\mathrm{HR}}$, with the fluctuations computed through Reynolds decomposition:

$$\mathbf{u}'_{\mathrm{LR}}(\mathbf{x}, t) = \mathbf{u}_{\mathrm{LR}}(\mathbf{x}, t) - \overline{\mathbf{u}_{\mathrm{LR}}(\mathbf{x}, t)}^{t} = \sum_{i=1}^{N} \boldsymbol{\phi}_i(\mathbf{x})\,\alpha_i(t)\,. \tag{31}$$

The POD procedure applied to $\mathbf{u}'_{\mathrm{LR}}(\mathbf{x}, t)$ provides a set $\{\boldsymbol{\phi}_i(\mathbf{x}), i \in [1, N]\}$ of eigenfunctions that are stationary in time and such that

$$\langle \boldsymbol{\phi}_m, \boldsymbol{\phi}_n \rangle = \int_{\Omega} \boldsymbol{\phi}_m^{\mathrm{T}} \boldsymbol{\phi}_n(\mathbf{x})\,\mathrm{d}\mathbf{x} = \delta_{mn}, \quad \overline{\alpha_m \alpha_n}^{t} = \lambda_m \delta_{m,n}. \tag{32}$$

The eigenfunctions are used to define the random field and a stationary variance tensor as

$$\boldsymbol{\sigma}\,\mathrm{d}\mathbf{B}_t(\mathbf{x}) = \sum_{i=1}^{M(z)} \lambda_i^{1/2} \boldsymbol{\phi}_i(\mathbf{x}) \sqrt{\Delta t}\,\mathrm{d}\beta_t^i, \qquad \mathbf{a}(\mathbf{x}) = \sum_{i=1}^{M(z)} \lambda_i \Delta t\, \boldsymbol{\phi}_i(\mathbf{x}) \boldsymbol{\phi}_i^{\mathrm{T}}(\mathbf{x}) \tag{33}$$

where $\boldsymbol{\varphi}_i = \boldsymbol{\phi}_i \sqrt{\Delta t}$ and $M(z) \ll N$ chosen to provide at least 85% of the energy of the fluid layer. Due to the constraint posed by Eq. (26) on the noise, incompressibility on the horizontal noise is imposed by applying a Helmoltz-Hodge decomposition [19] on the each snapshot of the horizontal velocity $\mathbf{u}_{\mathrm{LR}}$. Moreover, the set of eigenfunctions $\{\boldsymbol{\phi}_i(\mathbf{x}), i \in [1, N]\}$ is used to construct the drift $\boldsymbol{\mu}_t$ of Eq. (4) in such a way that the distance between $\boldsymbol{\mu}_t$ and $\overline{\mathbf{u}_{\mathrm{LR}}}^{t}$ is minimized, that is

$$\boldsymbol{\mu}_t = \sum_{i=1}^{N} \boldsymbol{\phi}_i(\mathbf{x})\, y_t^i \quad \text{with} \quad y_t^i = \arg\min \left\| \overline{\mathbf{u}_{\mathrm{LR}}(\mathbf{x}, t)}^{t} - \sum_{i=1}^{N} \boldsymbol{\phi}_i(\mathbf{x})\, y_t^i \right\|_2 . \tag{34}$$

Due to the orthogonality of the basis functions the coefficients can be easily recovered as the orthogonal projection $y_t^i = \langle \overline{\mathbf{u}_{\mathrm{LR}}(\mathbf{x}, t)}^{t}, \boldsymbol{\phi}_i(\mathbf{x}) \rangle$.

6 Results

In this work we focus on the results of a single realisation. From a qualitative point of view, the effect of the coarsening of the resolution can be seen in Figs. 1 and 2, where the leftmost panel represents the result the R27d simulation, the central panel shows the results of the R3d simulation and the rightmost panel shows the R3LU simulation. The first noticeable characteristic of the R27d reference simulation is the presence of a primary jet stream inclined at an almost $-45°$ angle starting at the bottom-left corner and directed towards the centre, and a secondary, smaller jet with the same inclination roughly 80 km above the primary. The presence of both structures is visible in the reference papers [17, 18]. In both figures the comparison between the high resolution and the low resolution deterministic simulation shows a degradation of the information about the jet-streams. Figure 1, depicting the relative vorticity $\overline{\zeta}^{10\mathrm{Y}} = \overline{\left(\partial_x v - \partial_y u\right)/f}^{10\mathrm{Y}}$, shows that the deterministic R3d simulation is incapable of reproducing the primary jet characteristic and its positioning, though showing an increased activity in place of the secondary jet stream. The stochastic R3LU simulation presents instead a intensification of the vortical activity in the

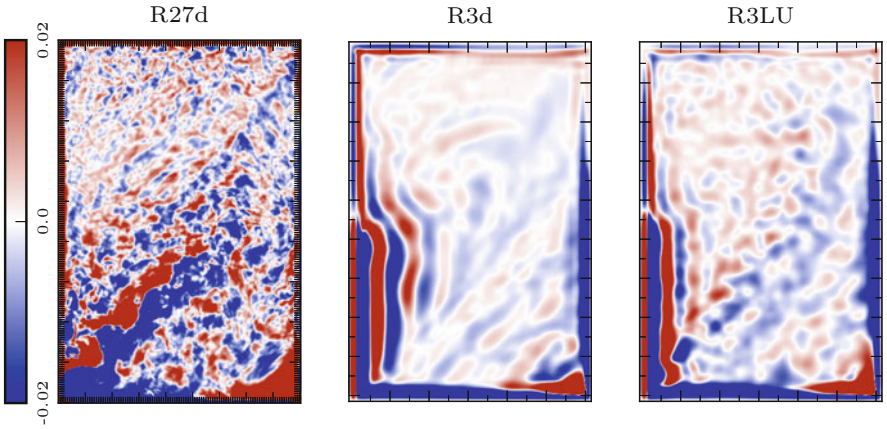

Fig. 1 10-years averaged relative vorticity $\zeta = \left(\partial_x v - \partial_y u\right)/f$ at the surface layer of the model for deterministic high-resolution (1/27°, left), for deterministic low resolution (1/3°, middle) and for stochastic low resolution (1/3°, right)

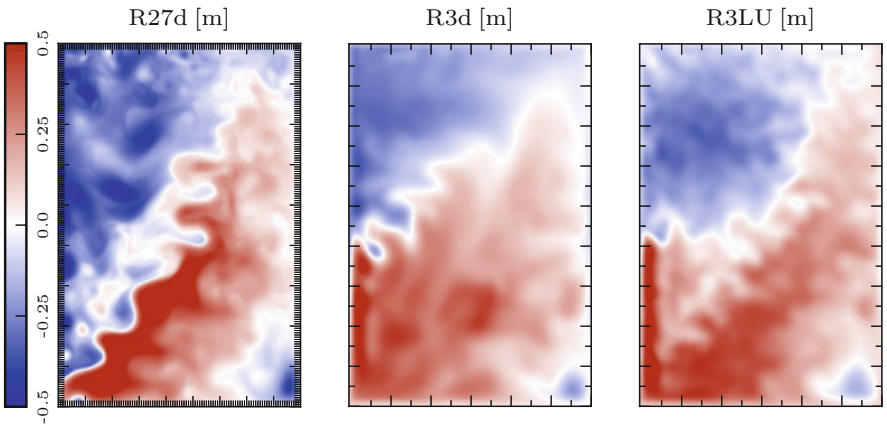

Fig. 2 5-days averaged sea surface height of the model for deterministic high-resolution (1/27°, left), for deterministic low resolution (1/3°, middle) and for stochastic low resolution (1/3°, right)

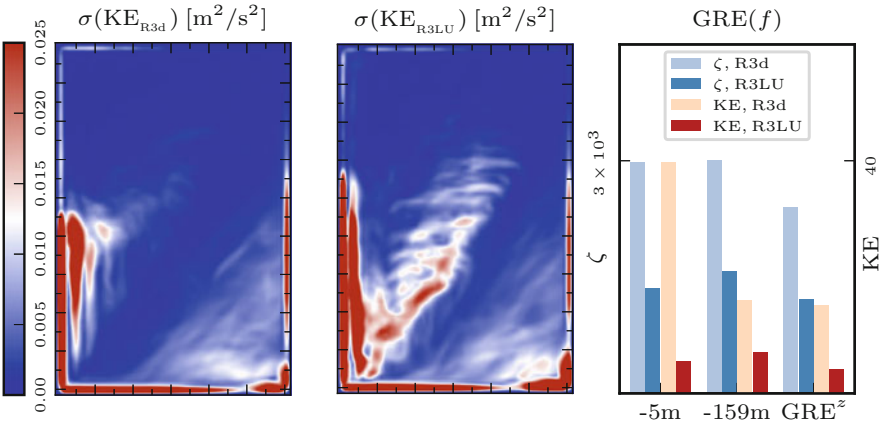

Fig. 3 Left and centre panels, standard deviation of the kinetic energy. The color scale has been adjusted to enhance the differences in the jet region, not considering the highly energetic boundaries where peaks present values as 0.2 m^2/s^2 for R3d and 0.17 m^2/s^2 for R3LU. Right panel, the Gaussian relative entropy for relative vorticity, ζ, (cold palette) and kinetic energy (warm palette). The lighter colors represent the deterministic simulation R3d, the darker colors represent the stochastic simulation R3LU. All the statistics are computed over 10 years

regions of the primary and secondary jet. Considering sea surface height, Fig. 2 shows that the best result is obtained by the stochastic simulation that, while not being able to distinguish the primary jet stream by the smaller vortices of the secondary jet, it is capable of reproducing the main behaviour. The left and centre panels of Fig. 3 shows the difference obtained in terms of variance of the kinetic energy in the two coarse simulations, with greater variability obtained with the stochastic model, especially in the area of the jet stream, where a lesser variability is

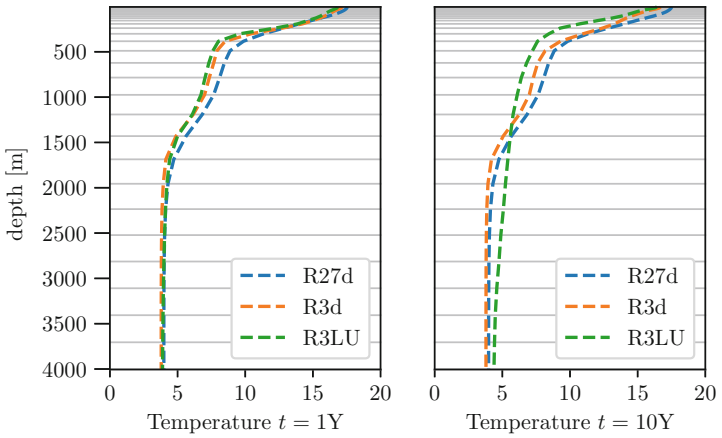

Fig. 4 Vertical profile of temperature after 1 year of simulation (left) and after 10 years (right)

shown in the deterministic case. From a quantitative point of view, the simulations are compared using the Gaussian Relative Entropy described in details in [20] and which measures with a single criterion both the mean and variance reconstructions. In the left panel of Fig. 3, values of the GRE for two variables, the relative vorticity ζ, and the kinetic energy $\mathrm{KE} = \left(u^2 + v^2\right)/2$ are compared. For two different depths and in a vertical average sense ($\overline{GRE}^z$), the relative entropy is smaller for the stochastic simulation, indicating a smaller distance from the distribution given by the reference R27d simulation. The proposed stochastic model thus outperforms the standard deterministic simulation in terms of both relative entropy and intrinsic variability for kinetic energy and vorticity. This behaviour is observed in every layer. In the tracers equation the noise has been scaled with the aid of the Schmidt number, the ratio between the eddy viscosity and eddy diffusivity. This consideration stems from the fact that the correlation times for transport of momentum and of tracers are not the same, and the difference can be expressed in terms of the Schmidt number. Figure 4 shows the vertical profiles of horizontally-averaged temperature, $\overline{T}^{x,y}(z,t) = \int_A T(x,y,z,t)\,\mathrm{d}x\mathrm{d}y$, at time $t = 1$Y and $t = 10$Y for the three simulations. The vertically averaged temperature shows an increase in mixing of temperature of the stochastic setting with respect to its deterministic counterparts. This process has been observed to be sensible to the noise amplitude and might be caused by the structure of the noise and by the effects of Helmholtz-Hodge decomposition. Further studies to investigate this process with three-dimensional and isopycnal noise are ongoing.

7 Conclusions

The considered stochastic model has been implemented into the NEMO dynamical core. A 3D horizontal, incompressible noise was considered and has been proven to successfully increase the capabilities of a coarse simulation in simulating the dynamical quantities of interest, when corrected with a stochastic drift leading to a change of probability measure. Both the qualitative behaviour of the jet-stream and the quantitative intrinsic variability of the model have been increased. Thermodynamic quantities like temperature and salinity seem to not benefit from this implementation. In future works, more complex non stationary fully 3D noises will be investigated within the same setting.

Acknowledgments The authors acknowledge the support of the ERC EU project 856408-STUOD.

References

1. Mémin, E: Fluid flow dynamics under location uncertainty. Geophysical and Astrophysical Fluid Dynamics 108, 119–197 (2014).
2. Holm, D. D.: Variational principles for stochastic fluid dynamics. Proceedings of the Royal Society A: Mathematical, Physical and Engineering Sciences, 471(20140963), 2015.
3. Chapron, B., Dérian, P., Mémin, E., Resseguier, V.: Large-scale flows under location uncertainty: a consistent stochastic framework. QJRMS, 144(710):251–260, 2018.
4. Bauer, W., Chandramouli, P., Chapron, B., Li, L., Mémin, E.: Deciphering the role of small-scale inhomogeneity on geophysical flow structuration: a stochastic approach. Journal of Physical Oceanography, (2020).
5. Resseguier , V., Mémin, E., Chapron, B.: Geophysical flows under location uncertainty, Part I Random transport and general models Geophysical and Astrophysical Fluid Dynamics 111, 149–176 (2017).
6. Cintolesi, C., Mémin, E.: Stochastic Modelling of Turbulent Flows for Numerical Simulations Fluids 5, (2020).
7. Kadri Harouna, S., Mémin, E.: Stochastic representation of the Reynolds transport theorem: Revisiting large-scale modelling. Computers and Fluids 156, 456–469 (2017).
8. Pinier, B., Mémin, E., Laizet, S., Lewandowski R.: Stochastic flow approach to model the mean velocity profile of wall-bounded flows. Phys. Rev. E, 99(6):063101, 2019.
9. Brecht, R., Li, L., Bauer, W., Mémin, E.: Rotating shallow water flow under location uncertainty with a structure-preserving discretization. J. of Advances in Modelling of Earth Systems, 13(12), 2021.
10. Heinrich, J.C., Huyakorn, P.S., Zienkewicz, O.C., Mitchell, A.R.: An 'Upwind' Finite Element Scheme for Two-dimensional Convective Transport Equation. International Journal for Numerical Methods in Engineering 11, 131–143, (1977).
11. Holmes, P., Lumley, J. L., Berkooz, G.: Turbulence, coherent structures, dynamical systems, and symmetry. Cambridge University Press (1996).
12. Vallis, Geoffrey K.: Atmospheric and Oceanic Fluid Dynamics: Fundamentals and Large-Scale Circulation. Cambridge University Press, 2nd edition (2017).
13. Borisenko, A. I., Tarapov, I. E., Silverman, R. A.: Vector and Tensor Analysis with Applications. Dover Publications (1979).
14. Batchelor, G. K.: An Introduction to Fluid Dynamics. Cambridge University Press (2000)

15. Kunita, H.: Stochastic Flows and Stochastic Differential Equations. Cambridge Studies in Advanced Mathematics (1997)
16. Madec, G., Bourdallé-Badie, R., Chanut, J., Clementi, E., Coward, A.,Ethé, C., Iovino, D., Lea, D., Lévy, C., Lovato, T., Martin, N., Masson, S., Mocavero, S., Rousset, C., Storkey, D., Vancoppenolle, M., Müller, S., Nurser, G., Bell, M., Samson, G.: Nemo ocean engine, Oct. 2019.
17. Lévy, M. , Klein, P., Tréguier, A.-M., Iovino, D. , Madec, G., Masson, S., Takahashi, K.: Modifications of gyre circulation by sub-mesoscale physics. Ocean Modelling, 34(1-2):1–15, 2010.
18. Lévy, M. Resplandy, L., Klein, P., Capet, X., Iovino, D., Ethé, C.: Grid degradation of submesoscale resolving ocean models: Benefits for offline passive tracer transport. Ocean Modelling, 48:1–9, 2012.
19. Denaro, F. M.: On the application of the helmholtz–hodge decomposition in projection methods for the numerical solution of the incompressible Navier–Stokes equations with general boundary conditions. International Journal for Numerical Methods in Fluids, 43:43–69, 09 2003.
20. Grooms, I., Majda, A., Smith, S.: Stochastic superparameterization in a quasi-geostrophic model of the antarctic circumpolar current. Ocean Modelling, 85, 10 2014.
21. Brecht, R. , Li, L., Bauer, W., Mémin, E.: Rotating shallow water flow under location uncertainty with a structure-preserving discretization. Journal of Advances in Modeling Earth Systems, American Geophysical Union, 2021, 13 (12)
22. Bauer, W., Chandramouli, P., Li, L., Mémin, E.: Stochastic representation of mesoscale eddy effects in coarse-resolution barotropic models Ocean Modelling, Elsevier, 2020, 151, pp.1–50.
23. Resseguier, V., Li, L., Jouan, G., Dérian, P., Mémin, E., Chapron, B.: New trends in ensemble forecast strategy: uncertainty quantification for coarse-grid computational fluid dynamics Archives of Computational Methods in Engineering, Springer Verlag, 2021, 28 (1), pp.215–261. https://doi.org/10.1007/s11831-020-09437-x
24. Loeve, M.: Probability theory, volume II. Springer, Graduate Texts in Mathematics (1978).